Supplementary Information

Low-temperature topotactic conversion growth of porous $CoFe_2O_4$ nanocubes for advanced oxygen evolution reaction

Linfeng Chen,[a] Zhenyuan Liu,*[a,b] Zhiyong Han,[a] Yuxiu Shi,[a] Jiale He,[a] Haoyang Chen,[a] Qicheng Liu,[c] and Yawen Tang*[b]

[a] School of Materials Science and Engineering, Jiangsu University of Science and Technology, Zhenjiang 212100, China. Email: zhenyuanliu@just.edu.cn (Z. Liu)

[b] Jiangsu Key Laboratory of New Power Batteries, Jiangsu Collaborative Innovation Centre of Biomedical Functional Materials, School of Chemistry and Materials Science, Nanjing Normal University, Nanjing 210023, China. E-mail: yawentang@njnu.edu.cn (Y. Tang)

[c] School of Food Science and Pharmaceutical Engineering, Nanjing Normal University, Nanjing 210023, China.

Experimental

Chemical and materials

Ferric chloride ($FeCl_3$), potassium hexacyanocobaltate (III) ($K_3Co(CN)_6$) and commercial ruthenium dioxide (RuO_2) were purchased from Aladdin Chemistry Co., Ltd (Shanghai, China). All materials were used without further purification. All the aqueous solutions were fixed with Millipore water at a resistivity of 18.2 MΩ.

Synthesis of porous $CoFe_2O_4$ nanocubes

In a standard synthesis, 20 mL of 50 mM $FeCl_3$ aqueous solution was mixed with 20 mL of 50 mM $K_3Co(CN)_6$ aqueous solutions under vigorous stirring for 5 min. Subsequently, the mixture was heated at 50 ℃ for 5 h and allowed to stand for 12 h to yield a pale yellow Fe-Co Prussian blue analogous (Fe-Co PBAs) precipitate. The precipitate was washed with ethanol and deionized water several times and separated by centrifugation at 9000 rpm for 5 min, and then dried at 40 ℃ for 12 h in a vacuum oven. The obtained dried Fe-Co PBAs were annealed at 320 ℃ for 1 h under air atmosphere with a heating rate of 1 ℃ min^{-1}. After being cooled down to room temperature, the resulting black products were washed three times by centrifugation with distilled water and ethanol, and then dried at 40 ℃ to obtain porous spinel oxide $CoFe_2O_4$ nanocubes ($CoFe_2O_4$ NCs).

Physical characterization

The morphology and structure of products were examined on JEOL JEM-2010 transmission electron microscope (TEM) and Hitachi S-4800 scanning electron microscopy (SEM). High-resolution transmission electron microscope (HRTEM), energy-dispersive X-ray (EDX), high-angle annular dark-field scanning transmission electron microscope (HAADF-STEM), and elemental mapping measurements were performed using FEI Tecnai G2 F20 microscope on the JEOL JEM-2100F. The Fourier transform infrared (FT-IR) spectra were recorded on a Nicolet 520 SXFTIR spectrometer. The phase purity and crystallinity of the products were identified by X-ray diffraction (XRD) on a Model D/max-rC X-ray diffractometer with Cu Kα radiation source (λ = 1.5406 Å) at 40 kV and 100 mA. X-ray photoelectron spectroscopy (XPS) measurements were conducted using a Thermo VG Scientific ESCALAB 250

spectrometer equipped with a monochromatic Al Kα X-ray source (1486.6 eV photons). All binding energies were calibrated against the C 1s at 284.6 eV. Thermogravimetric analysis (TGA) of the product was carried out with a Netzsch STA 449C thermal analyser at a heating rate of 10 ℃ min^{-1} under air atmosphere.

Electrochemical measurements

All electrochemical investigations were carried out using a CHI 760 E electrochemical workstation (CH Instruments, Chenhua Co., Shanghai, China) at 25 ℃ in a standard three-electrode configuration. The conventional three-electrode setup comprised a stone grinding rod auxiliary electrode, a saturated calomel electrode (SCE) as the reference electrode, and a working electrode consisting of a glassy carbon electrode coated with the catalysts. Cyclic voltammetry (CV) curve tests were obtained in N_2-saturated 1 M KOH solution. The OER tests were carried out in O_2-saturated 1 M KOH solution with a sweep rate of 5 mV s^{-1}. The electrochemical double-layer capacitance (C_{dl}) was determined using CV method within a non-Faradaic potential range (1.07-1.17 V) at different scan rates (40-200 mV s^{-1}). The electrochemical impedance spectroscopy (EIS) was tested over a frequency range of 100 kHz-0.1 Hz. All potentials were calibrated to reversible hydrogen electrode (RHE) in this work.

Figures and Tables

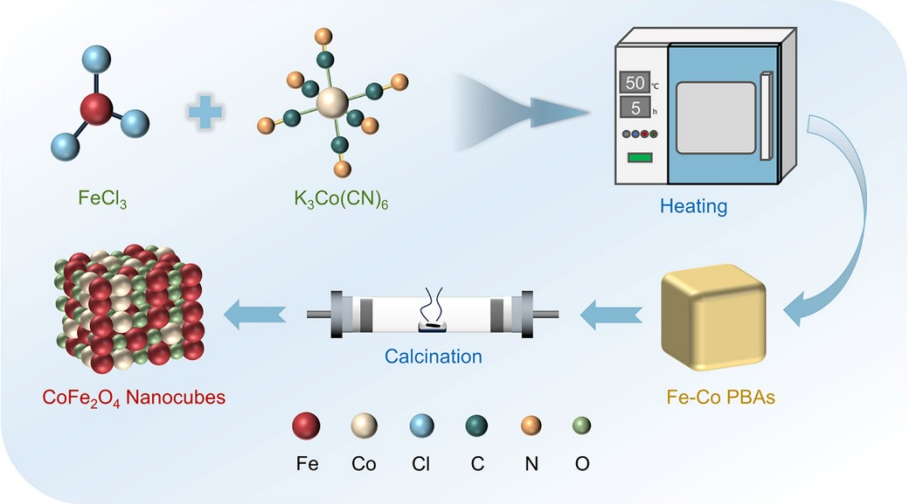

Fig. S1 Schematic illustration of the preparation of porous $CoFe_2O_4$ NCs.

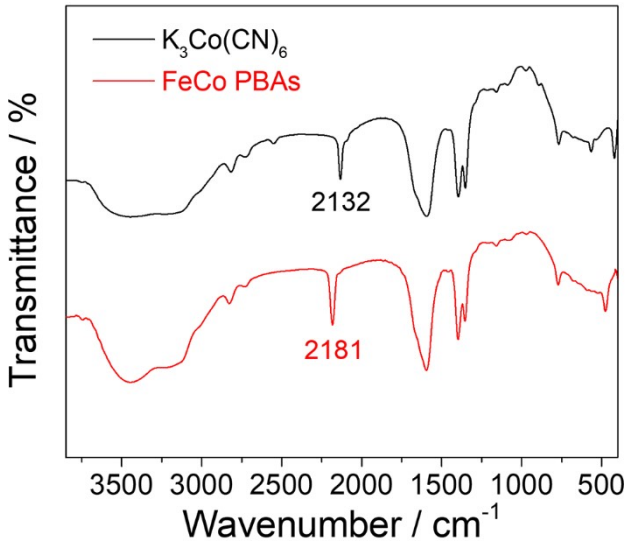

Fig. S2 FTIR spectra of Fe-Co PBAs and $K_3Co(CN)_6$.

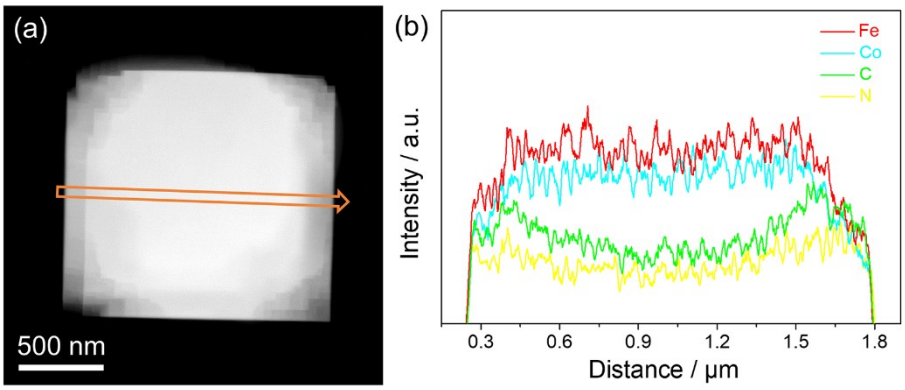

Fig. S3 (a) HAADF-STEM image and (b) EDX line scanning profile of the Fe-Co PBAs.

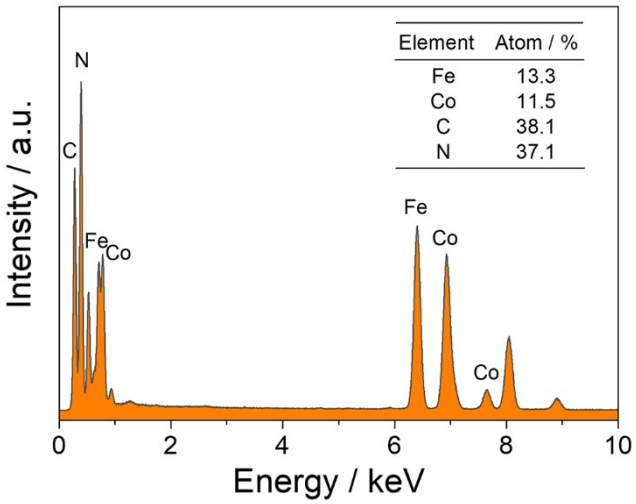

Fig. S4 EDX analysis of the Fe-Co PBAs.

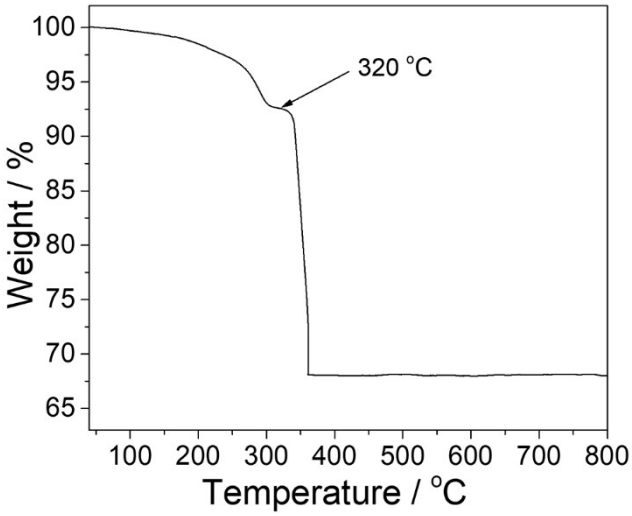

Fig. S5 TGA analysis of the Fe-Co PBAs.

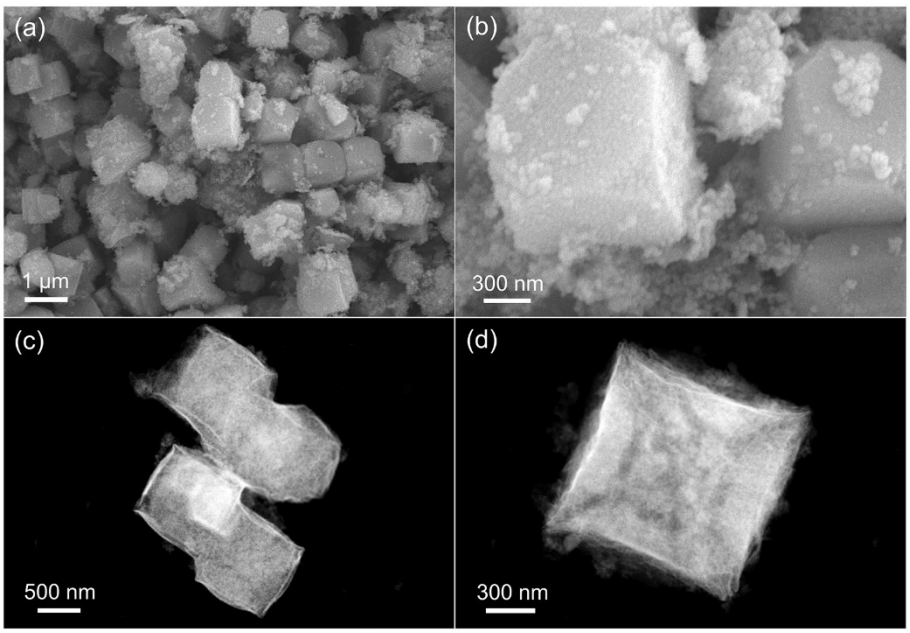

Fig. S6 (a-b) SEM and (c-d) HAADF-STEM images of the porous $CoFe_2O_4$ NCs.

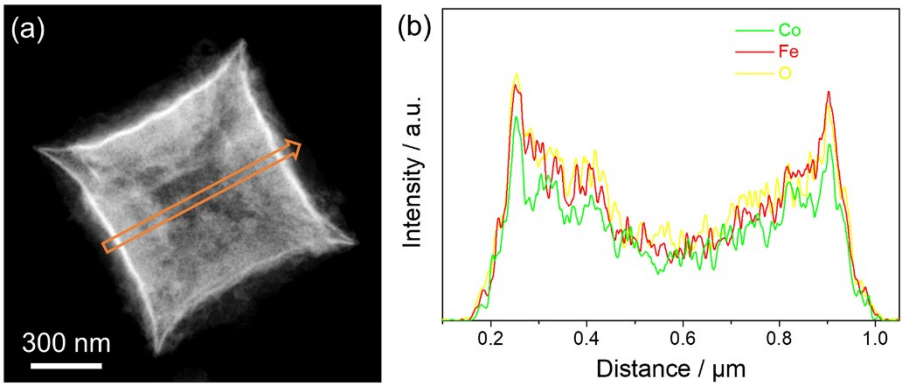

Fig. S7 (a) HAADF-STEM image and (b) EDX line scanning profile of the porous $CoFe_2O_4$ NCs.

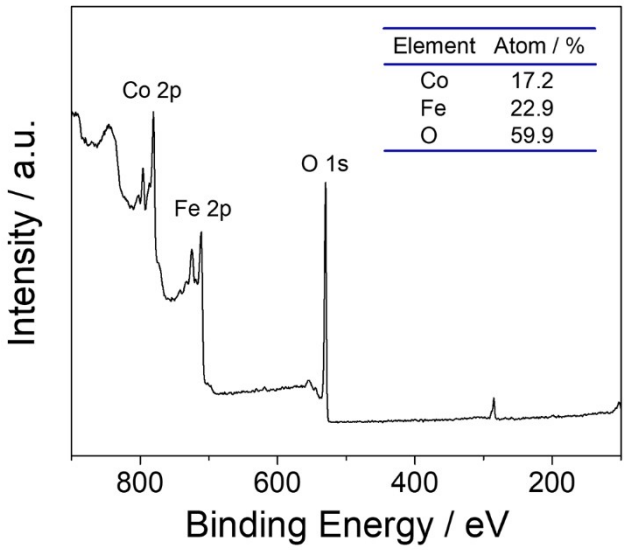

Fig. S8 XPS survey scan spectrum of the porous $CoFe_2O_4$ NCs.

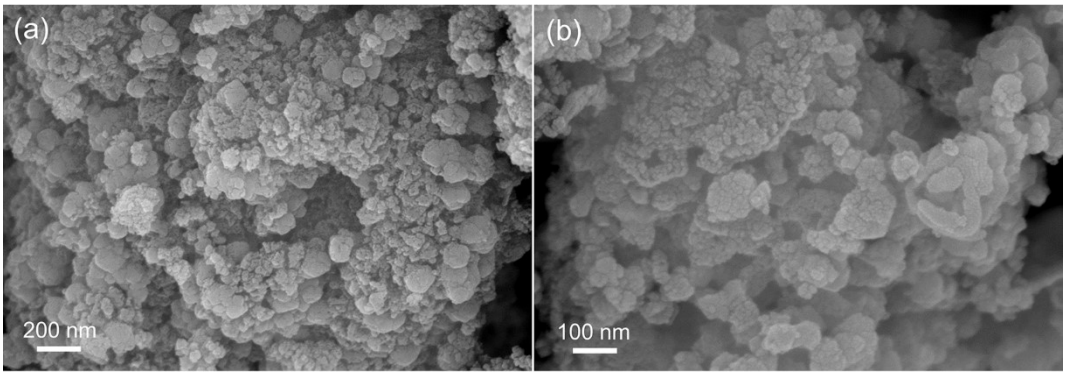

Fig. S9 SEM images of non-porous $CoFe_2O_4$.

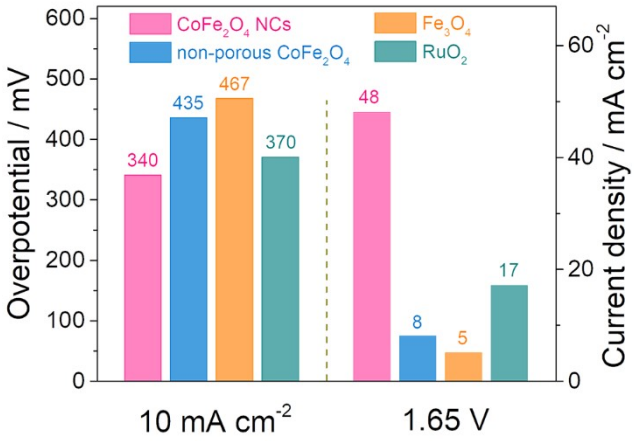

Fig. S10 Comparisons of overpotentials at 10 mA cm^{-2} and current densities at 1.65 V (*vs*. RHE) of porous $CoFe_2O_4$ NCs, non-porous $CoFe_2O_4$, Fe_3O_4, and RuO_2 catalysts.

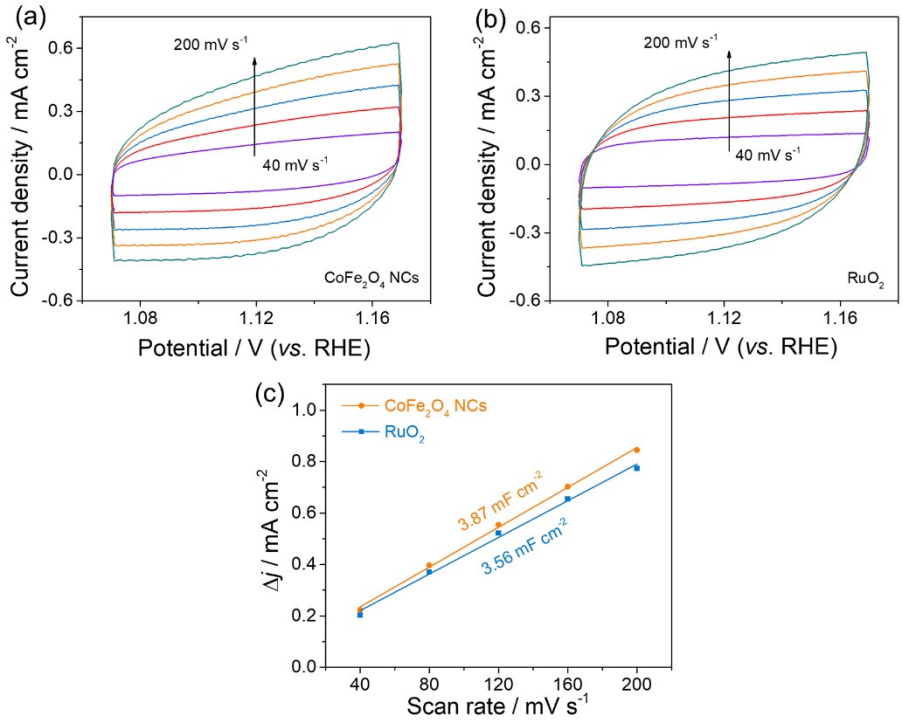

Fig. S11 CV curves at different scan rates of (a) the porous $CoFe_2O_4$ NCs and (b) RuO_2 catalysts. (c) C_{dl} values of the porous $CoFe_2O_4$ NCs and RuO_2 catalysts.

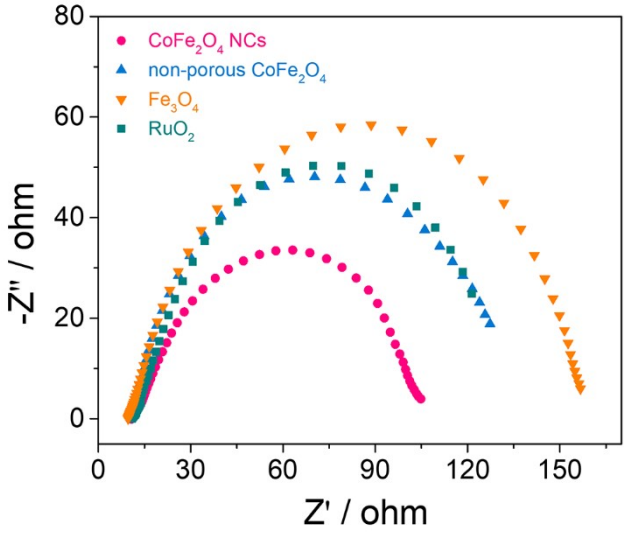

Fig. S12 EIS Nyquist plots of the $CoFe_2O_4$ NCs, non-porous $CoFe_2O_4$, Fe_3O_4, and RuO_2 catalysts.

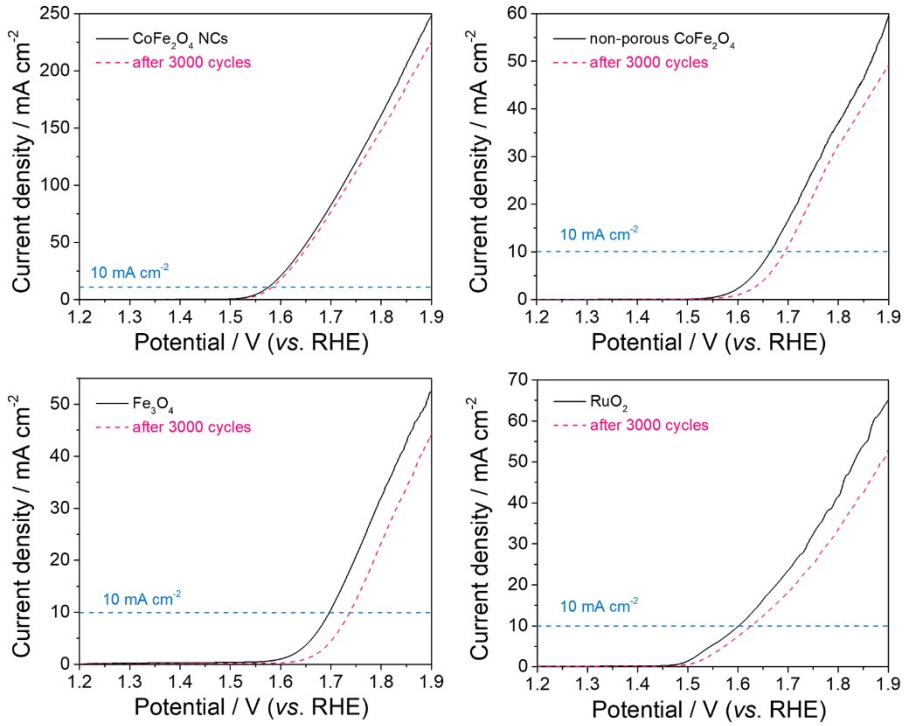

Fig. S13 OER polarization curves of the $CoFe_2O_4$ NCs, non-porous $CoFe_2O_4$, Fe_3O_4, and RuO_2 before and after 3000 cycles.

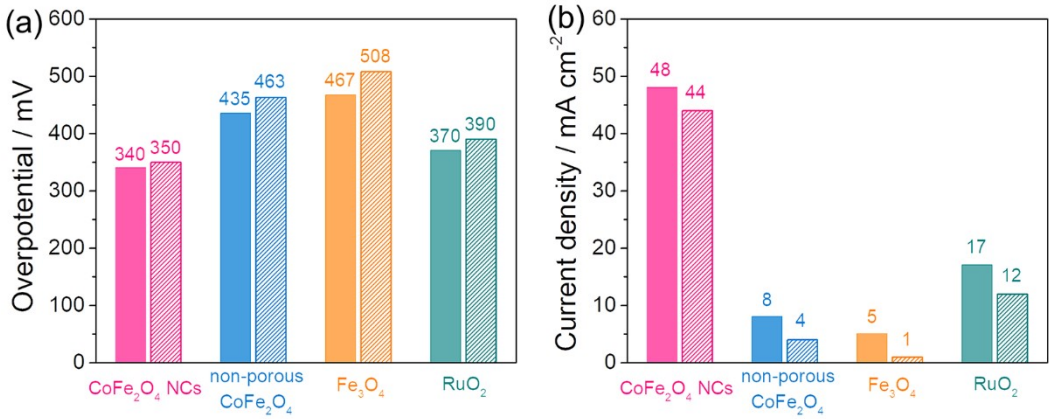

Fig. S14 Comparisons of (a) overpotentials at 10 mA cm^{-2} and (b) current densities at 1.65 V (*vs*. RHE) before and after 3000 cycles of porous $CoFe_2O_4$ NCs, non-porous $CoFe_2O_4$, Fe_3O_4, and RuO_2 catalysts.

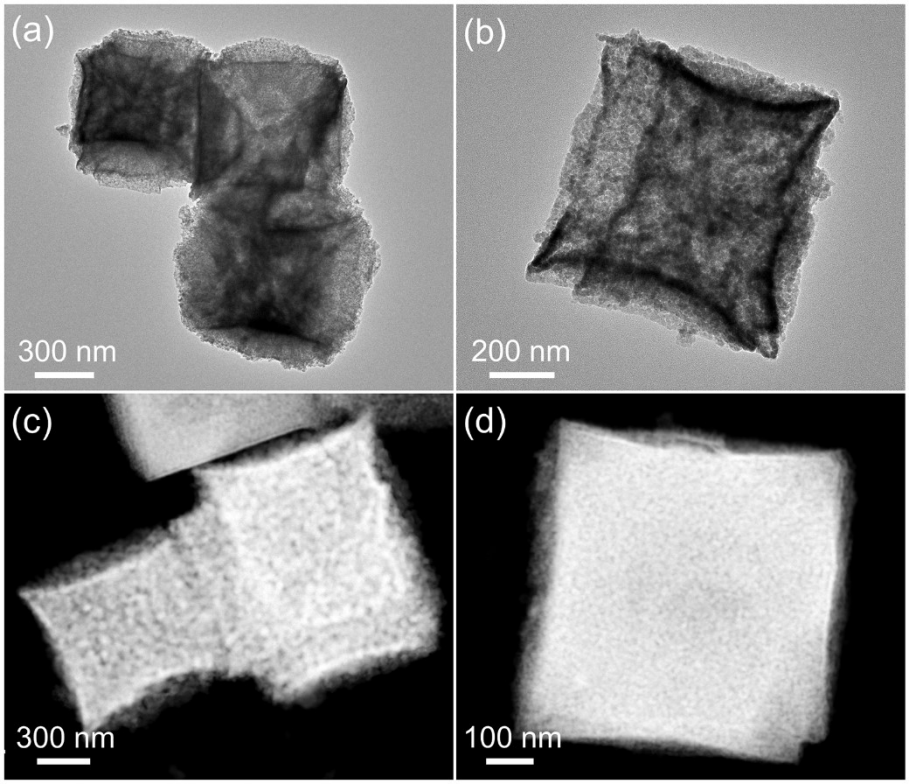

Fig. S15 (a-b) HRTEM and (c-d) HAADF-STEM images of the porous $CoFe_2O_4$ NCs after stability tests.

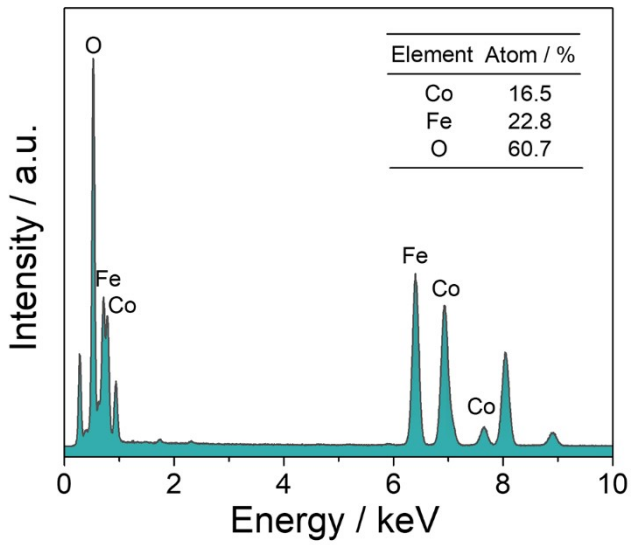

Fig. S16 EDX analysis of the porous $CoFe_2O_4$ NCs after stability tests.

Table S1. Comparison of the OER activity of porous $CoFe_2O_4$ nanocubes with other reported catalysts in 1 M KOH.

Catalyst	Overpotential / mV (10 mA cm^{-2})	Tafel plots / mV dec^{-1}	Ref.
$CoFe_2O_4$ nanocubes	**340**	**49.4**	**This work**
$ZnCo_2O_{4-x}F_x$/CNTs	350	59.2	Angew. Chem. Int. Ed. 2023, 62, e202301408.
Co_3O_4	350	/	Angew. Chem. Int. Ed. 2019, 58, 6042.
FeCo@NG/NCNT	450	77	New J. Chem. 2018, 42, 3409.
MoS_2/Co-N-CN_2-900°C	442	169	ACS Sustain. Chem. Eng. 2020, 8, 5724.
FeNi/NC/gC_3N_4/NF	350	95	Electrochim. Acta 2020, 331, 135375.
$NiCo_2O_4$/MXene Hybrid	360	64	ChemCatChem 2024, 16, e202301250.
Co-doped NiO	450	89	R. Soc. Open Sci. 2021, 8, 202352.
P-$NiCo_2O_4$	370	95	Mater. Today Commun. 2022, 31, 103708.
$CoFe_2O_4$	359	53.8	Electrochim. Acta 2021, 395, 139195.
$NiCo_2O_4$/Ti	353	61	Int. J. Hydrog. Energy 2021, 46, 10259.